

Swapping exchange and spin-orbit induced correlated phases in ex-so-tic van der Waals heterostructures

Yaroslav Zhumagulov^{1,*}, Denis Kochan^{2,1,†} and Jaroslav Fabian^{1‡}

¹*Institute for Theoretical Physics, University of Regensburg, 93040 Regensburg, Germany*

²*Institute of Physics, Slovak Academy of Sciences, 84511 Bratislava, Slovakia*

(Dated: August 1, 2023)

Ex-so-tic van der Waals heterostructures take advantage of the electrically tunable layer polarization to swap proximity exchange and spin-orbit coupling in the electronically active region. Perhaps the simplest example is Bernal bilayer graphene (BBG) encapsulated by a layered magnet from one side and a strong spin-orbit material from the other. Taking WS₂/BBG/Cr₂Ge₂Te₆ as a representative ex-so-tronic device, we employ realistic *ab initio*-inspired Hamiltonians and effective electron-electron interactions to investigate the emergence of correlated phases within the random phase approximation. We find that for a given doping level, exchange and spin-orbit coupling induced Stoner and intervalley coherence instabilities can be swapped, allowing to explore the full spectrum of correlated phases within a single device.

Introduction. While a variety of novel electronic correlation effects have initially been discovered in twisted graphene structures [1–4], recent demonstrations of quarter and half-metallic states [5–10] and superconductivity [7, 11–17] in rhombohedral trilayer graphene, as well as the observation of isospin magnetism and spin-polarized superconductivity in Bernal bilayer graphene (BBG) [18–26], are a clear evidence for correlated physics without moiré patterns. The common feature, boosting the electron-electron interactions in these systems, is the presence of van Hove singularities (vHS) near the charge neutrality point [27–29]. Particularly attractive is the tunability of the correlated phases by a displacement field, which can shift the electronic levels of the vHS. [5, 11, 18, 19].

The electronic states of 2D materials in van der Waals heterostructures can be also affected by proximity effects [30]. Relatively strong spin interactions, for example, can be induced in materials such as graphene which exhibits weak spin-orbit coupling [31–33]. Indeed, proximity-induced spin-orbit (SO) and exchange (EX) interactions have been predicted theoretically [34–45] and confirmed experimentally [46–57] in BBG-based heterostructures. Specifically, valley-Zeeman, Kane-Mele, and Rashba SO couplings have been shown to emerge [34–41, 46–56], along with (anti)ferromagnetic EX couplings [39–43, 45, 56–58], typically causing spin splittings on the meV scale.

Perhaps the most striking manifestation of the proximity effects is the possibility to swap the spin couplings, EX and SO, by a displacement field, whereby changing the spin Hamiltonian in the active layer. This effect arises due to the interplay of the short-range proximity interactions and layer polarization by the field. An experimentally relevant materials system to consider is that of BBG encapsulated from one side by a strong spin-orbit material, such as WS₂, and a magnetic semiconductor, such as Cr₂Ge₂Te₆ (CGT), from the other side. The resulting heterostructure, termed ex-so-tic [40], allows to

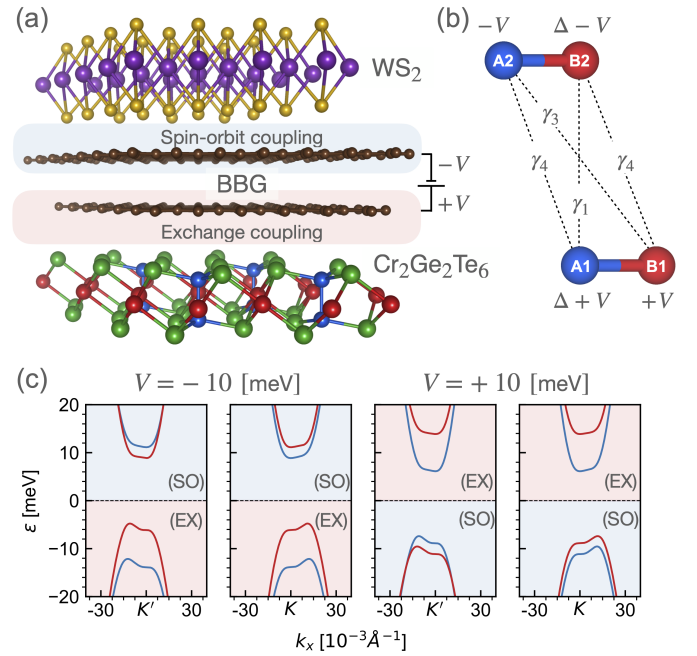


FIG. 1. (a) Scheme of an ex-so-tic heterostructure comprising BBG encapsulated by WS₂ and CGT which proximitize the BBG by SO (WS₂) and EX (CGT) interactions. (b) BBG unit cell with relevant interlayer orbital hoppings and on-site energies. The intralayer nearest-neighbor hopping γ_0 is not indicated. The colors distinguish A and B sublattices within the two layers. (c) Calculated single-particle low-energy electronic dispersions of WS₂/BBG/CGT near K and K' points obtained from $h(\mathbf{k}, \tau)$ for $V = \pm 10$ meV; red bands are spin-polarized up, and blue are spin-polarized down; the spin quantization axis z is perpendicular to the layers.

imprint selectively either SO or EX coupling onto the Bloch states of the BBG.

Given that BBG can host correlated phases, is it possible to swap between the phases induced by EX and SO coupling? As we show here, ex-so-tronic devices

can indeed supply on-demand correlated phases, allowing to swap the effective single-particle excitation Hamiltonians enabled by the layer polarization effect. Although our conclusions are more general, we specifically study WS₂/BBG/CGT, for which an effective orbital and spin-interaction Hamiltonian has been derived from DFT [39, 40]. Employing random-phase approximation (RPA) [59–64], we first examine the particle-hole instabilities of pristine BBG, whose correlated phase diagram features intervalley coherence (IVC) [65] and Stoner instabilities [14, 15]. The spin interactions induced by proximity SO (see the latest works [26, 66–68]) and EX couplings remove the spin and valley degeneracies of IVC and Stoner phases and cause a plethora of emergent spin-valley correlated phases. In ex-so-tic heterostructures, such as in here employed WS₂/BBG/CGT, the phases can be effectively swapped, while the evidence of the interplay of SO and EX interactions can be seen in the single-particle (Hartree-Fock) excitation spectra which we also calculate.

Model. The orbital degrees of freedom of BBG are modeled by a realistic Bloch Hamiltonian [32, 40]:

$$\hat{h}_0(\mathbf{k}, \tau) = \begin{pmatrix} \Delta + V & \gamma_0 f(\mathbf{k}) & \gamma_4 f^*(\mathbf{k}) & \gamma_1 \\ \gamma_0 f^*(\mathbf{k}) & +V & \gamma_3 f(\mathbf{k}) & \gamma_4 f^*(\mathbf{k}) \\ \gamma_4 f(\mathbf{k}) & \gamma_3 f^*(\mathbf{k}) & -V & \gamma_0 f(\mathbf{k}) \\ \gamma_1 & \gamma_4 f(\mathbf{k}) & \gamma_0 f^*(\mathbf{k}) & \Delta - V \end{pmatrix} \quad (1)$$

in the basis of p_z orbitals ordered as (A_1, B_1, A_2, B_2) . Parameters γ denote intra- (γ_0) and interlayer ($\gamma_1, \gamma_3, \gamma_4$) hoppings, see Figs. 1 (b) and (c). Displacement field is accounted for by on-site energy V , while the asymmetry between A and B sublattice is quantified by Δ . Momenta $\mathbf{k} = (k_x, k_y)$ are measured from K and K' valleys, while, $f(\mathbf{k}) = -(\sqrt{3}a/2)(\tau_x - ik_y)$ is the linearized nearest-neighbor tight-binding function; $a = 2.46 \text{ \AA}$ is graphene's lattice constant and $\tau = \tau_{K/K'} = \pm 1$ is the valley index. Since the SO coupling of pristine BBG is weak—about $24 \mu\text{eV}$ [32]—we do not include it in the Hamiltonian.

To model proximitized BBG in a WS₂/BBG/CGT ex-so-tic heterostructure we need to include SO (due to WS₂) and EX (due to CGT) couplings, which were shown by *ab initio* calculations and weak-antilocalization measurements [69] to be sizeable, on the order of 1 meV [39, 40]. The corresponding proximity induced spin interactions are described near K and K' valleys by the Hamiltonian $\hat{h}_{\text{prox}}(\tau) = \sum_l \hat{h}_{\text{vz}}^l(\tau) + \hat{h}_{\text{ex}}^l(\tau)$, for valley-Zeeman (vz) spin-orbit and exchange (ex) coupling [34, 38, 41, 44]:

$$\hat{h}_{\text{vz}}^l(\tau) = \begin{pmatrix} \tau \lambda_{\text{vz}}^{A_l} s_z & 0 \\ 0 & -\tau \lambda_{\text{vz}}^{B_l} s_z \end{pmatrix}, \quad (2)$$

$$\hat{h}_{\text{ex}}^l(\tau) = \begin{pmatrix} -\lambda_{\text{ex}}^{A_l} s_z & 0 \\ 0 & -\lambda_{\text{ex}}^{B_l} s_z \end{pmatrix}, \quad (3)$$

parameterized by the corresponding sublattice and layer-resolved couplings $\lambda_{\text{vz}}^{A_l/B_l}$ and $\lambda_{\text{ex}}^{A_l/B_l}$. We denote by s_z

the spin Pauli matrix. Each \hat{h}^l is a 4×4 matrix in the spin-sublattice resolved basis $(A_{l\uparrow}, A_{l\downarrow}, B_{l\uparrow}, B_{l\downarrow})$ within layer l (bottom is $l = 1$, top $l = 2$). Since spin-orbit coupling in graphene induced by TMDCs is of the valley-Zeeman type [37], we set $\lambda_{\text{vz}}^{A_l} \approx -\lambda_{\text{vz}}^{B_l}$.

The numerical values for the parameters of the single-particle Hamiltonian, $\hat{h}(\mathbf{k}, \tau) = \hat{h}_0(\mathbf{k}, \tau) + \hat{h}_{\text{prox}}(\tau)$, are taken from the *ab initio* results of Ref. [40]. The calculated low-energy band dispersions for WS₂/BBG/CGT are shown in Fig. 1(c). The signs of V and electron doping n_e determine the dominant proximity spin interaction. If both V and n_e positive or negative, the electrons at the Fermi level experience proximity exchange coupling, while if the signs of V and n_e are opposite, the electrons at the Fermi level have strong proximity spin-orbit coupling; we use labels (SO) and (EX) in Fig. 1(c) and below when needed to keep track of the dominant spin interaction.

To investigate correlation phenomena we introduce the many-particle Hamiltonian operator as the sum of the kinetic and potential energies $\hat{H} = \hat{H}_{\text{kin}} + \hat{H}_{\text{int}}$, where

$$\hat{H}_{\text{kin}} = \sum_{\mathbf{k}\tau s, ij} \hat{c}_{s\tau i}^\dagger(\mathbf{k}) \left[\hat{h}(\mathbf{k}, \tau) - \mu \right]_{si, s'j} \hat{c}_{s'\tau j}(\mathbf{k}), \quad (4)$$

$$\hat{H}_{\text{int}} = U_0 (\hat{n}_{\uparrow K} \hat{n}_{\downarrow K} + \hat{n}_{\uparrow K'} \hat{n}_{\downarrow K'}) + U_1 \hat{n}_K \hat{n}_{K'}. \quad (5)$$

Here, $\hat{c}_{s\tau i}^{(\dagger)}(\mathbf{k})$ is the annihilation (creation) operator for a Bloch electron with spin $s = \uparrow / \downarrow$ in valley $\tau = K/K'$ on BBG sublattice i with valley-momentum \mathbf{k} ; μ is the chemical potential. The intra- and intervalley density interactions are described by repulsive (positive) couplings U_0 and U_1 , respectively, while $\hat{n}_{s\tau} = \sum_{|\mathbf{k}| < k_c} \sum_i \hat{c}_{s\tau i}^\dagger(\mathbf{k}) \hat{c}_{s\tau i}(\mathbf{k})$ stands for the spin-valley number operator in the $s\tau$ -channel cut-off by a momentum k_c ; the valley number operator then is $\hat{n}_\tau = \hat{n}_{\uparrow\tau} + \hat{n}_{\downarrow\tau}$.

In the following, we consider SU(4)-symmetric interactions by setting $U_0 = U_1 = U = 19 \text{ eV}$ [14, 68, 70], and $k_c = 0.06 \text{ \AA}^{-1}$, which are consistent with the experimental pristine BBG phase diagram [18, 19]. We use the same interaction parameters for the WS₂/BBG/CGT heterostructure.

Methodology. To resolve the correlated phases of our models of pristine and proximitized BBG we employ the RPA. First, we evaluate the non-interacting generalized static Lindhard's susceptibility, χ^0 , [62–64, 71] using the BBG Hamiltonian \hat{H}_{kin} , Eq. (4), at 0.4 K , considering different spin-valley modes $s\tau$ in the particle-hole channel. Second, we calculate the dressed susceptibility, $\chi = [1 - \chi^0 \Gamma]^{-1} \chi^0$, where Γ is the irreducible vertex function corresponding to \hat{H}_{int} , Eq. (5). Finally, we check for divergence of χ : If the highest eigenvalue λ_c of $\chi^0 \Gamma$ becomes greater or equal to unity, a correlated phase corresponding to that eigenvalue emerges.

In particular, we find all possible correlated phases $\hat{\Phi}$ of different spin-valley channels by first diagonalizing $\chi^0 \Gamma$

pristine BBG phases	IVC		Stoner	
proximity phases	SVC $_{\pm}$	CDW $_{\pm}$	SVP $_{\pm}$	VP $_{\pm}$
spin-valley matrices M_{Φ}	$[s_x\tau_x \pm s_y\tau_y]$	$[s_0 \pm s_z]\tau_x$	$[s_z\tau_0 \pm s_0\tau_z]$	$[s_0 \pm s_z]\tau_z$

TABLE I. List of phases and corresponding phase operators $\hat{\Phi} = \sum_{|\mathbf{k}| < k_c} \sum_i \hat{c}_{s\tau i}^{\dagger}(\mathbf{k}) [M_{\Phi}]_{s\tau, s'\tau'} \hat{c}_{s'\tau' i}(\mathbf{k}) = \hat{\Phi}^{\dagger}$ resolved in different spin-valley channels for the relevant symmetry-broken phases of pristine and proximitized BBG. The spin-valley resolved matrices M_{Φ} entering $\hat{\Phi}$'s are given in the third line. Phases involving τ_x or τ_y are valley mixed, i.e., they possess spatial modulation with vector $\mathbf{q} = (2\pi/3a)(1, \sqrt{3})$ which connects K and K' valleys.

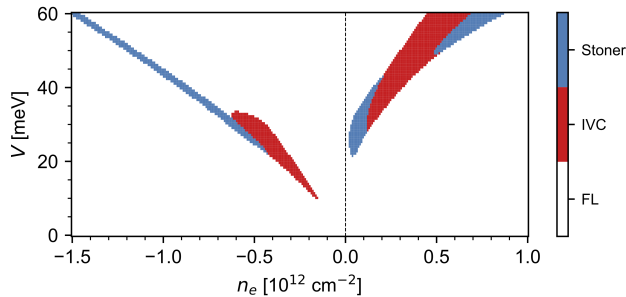


FIG. 2. Calculated phase diagram of pristine BBG for varying doping n_e and displacement field V . We only show phases for $V > 0$, as the diagram has V to $-V$ symmetry. There are two dominant phases: the intervalley coherent phase (IVC), displayed by blue, and the Stoner instability, shown in red. The white background corresponds to a stable Fermi liquid (FL).

at $\mu = 0$ and $V = 0$. Then, varying the doping and displacement field, we compute the corresponding χ^0 and $\chi^0\Gamma$. For each $\hat{\Phi}$ found above we estimate the critical parameter $\lambda_c(\hat{\Phi}) = \langle \hat{\Phi} | \chi^0\Gamma | \hat{\Phi} \rangle / \|\hat{\Phi}\|^2$. The dominant instability is realized by phase $\hat{\Phi}$ that at given μ and V has the highest $\lambda_c(\hat{\Phi})$. Each symmetry-breaking phase $\hat{\Phi}$ can be expressed in terms of $\hat{c}_{s\tau i}^{(\dagger)}(\mathbf{k})$ operators,

$$\hat{\Phi} = \sum_{|\mathbf{k}| < k_c} \sum_i \hat{c}_{s\tau i}^{\dagger}(\mathbf{k}) [M_{\Phi}]_{s\tau, s'\tau'} \hat{c}_{s'\tau' i}(\mathbf{k}), \quad (6)$$

where the spin-valley resolved matrices M_{Φ} that are relevant for our model are listed in Table I. However, at the phase boundaries, the dominant phase can be unresolved due to the degeneracy of several $\lambda_c(\hat{\Phi})$.

Figure 2 displays the obtained correlated phase diagram of pristine BBG. We find IVC and Stoner instabilities, as also reported earlier [14, 15]. While the Stoner instability is local, the IVC state corresponds to a phase spatially modulated by wave vector $\mathbf{q} = (2\pi/3a)(1, \sqrt{3})$ which connects K and K' valleys. The fact that \hat{H}_{kin} lacks particle-hole symmetry is reflected in the different phases for the electron and hole doping ranges. Both IVC and Stoner phases exhibit degeneracies, as listed in Table I, due to not fully broken spin-valley symmetries.

Figure 3 shows the main result of the paper. There, we plot the correlated phase diagram of $\text{WS}_2/\text{BBG}/\text{CGT}$

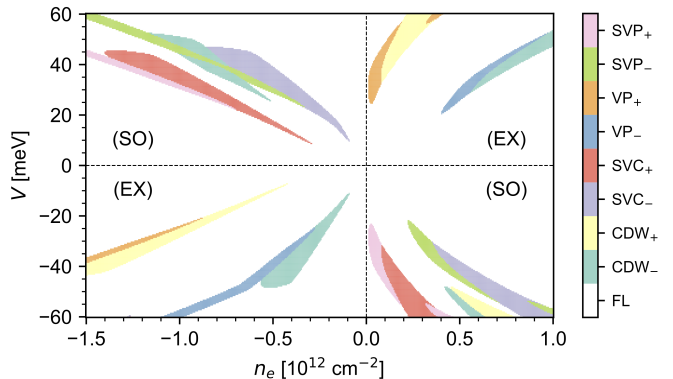


FIG. 3. (a) Correlated-phase diagram of a model ex-sotic $\text{WS}_2/\text{BBG}/\text{CGT}$ heterostructure, for varying doping n_e and displacement field V . Eight symmetry-breaking phases are predicted to emerge due to the interplay of the electron-electron interactions and proximity-induced SO and EX splittings: CDW $_{\pm}$ (charge density wave), SVC $_{\pm}$ (spin-valley coherence), SVP $_{\pm}$ (spin-valley polarized state), and VP $_{\pm}$ (valley polarized state), each marked by a different color. The stable Fermi liquid phase is displayed by white.

for different doping levels and displacement fields. Compared with the pristine case, the phase diagram of proximitized BBG is rather rich. Indeed, if the Fermi level crosses bands experiencing strong proximity SO coupling, the Stoner phase breaks up into two SVP $_{\pm}$ states—both displaying spin-valley polarization along the $\pm z$ direction—while IVC splits into spin-valley coherent states SVC $_{\pm}$. Resolving specific spin-valley states within the Stoner and IVC phases is attributed to the valley-Zeeman SO coupling [37]. Similarly, if the Fermi level lies in bands which have strong EX coupling, the Stoner phase evolves into valley-polarized states, VP $_{\pm}$, while IVC is split into charge density waves, CDW $_{\pm}$. The multitude of spin-valley-split phases of proximitized BBG due to SO and EX interactions is summarized in Table I, including the explicit forms of the phase operators $\hat{\Phi}$. Their expectation values in the corresponding ground states can serve as the conventional order parameters discriminating different phases.

Let us take a closer look at vHS. If the singularity is split due to the valley-Zeeman SO coupling, two SVC $_{\pm}$ phases appear. As the corresponding $M_{\text{SVC}_{\pm}}$ contain spin s_x and s_y matrices, and valley τ_x and τ_y matrices,

they can be described as inter-valley spin-flip hopping that retains the spin-valley quantum number, i.e., the product of $s\tau$. Say, spin up at K is degenerate with spin down at K' . Coupling the two enabled by the Coulomb interaction lowers the kinetic energy, resulting in an SVC correlated phase. Similarly, when vHS are split by EX interaction, two spin-polarized CDW $_{\pm}$ phases form up. Contrary to SVC $_{\pm}$, $M_{\text{CDW}_{\pm}}$ does not mix spins—it involves s_0 and s_z spin matrices—but similarly as SVC $_{\pm}$ it intertwines the valleys—matrix τ_x . Because of that both SVC $_{\pm}$ and CDW $_{\pm}$ possess spatial modulations governed by wave vector $\mathbf{q} = \frac{2\pi}{3a}(1, \sqrt{3})$; the correlations effectively enlarge the BBG unit cell into a “magnetic” $\sqrt{3} \times \sqrt{3}$ -unit cell. As a consequence, the Brillouin zone gets smaller, while both valleys fold into the Γ point. In what follows the \mathbf{k} vector is measured with respect to the centre of such the reduced Brillouin zone.

Finally, to find the effective single-particle excitation energies of the correlated phases of our WS $_2$ /BBG/CGT model we employ the Hartree-Fock (HF) method and solve the following eigen-problem:

$$\left(\hat{H}_{\text{kin}} + \hat{\Sigma}\right) |\tilde{u}_n(\mathbf{k})\rangle = \tilde{\varepsilon}_{n\mathbf{k}} |\tilde{u}_n(\mathbf{k})\rangle, \quad (7)$$

where $\tilde{\varepsilon}_{n\mathbf{k}}$ and $|\tilde{u}_n(\mathbf{k})\rangle$ are HF-corrected quasi-particle energies and wave-functions labelled by the band index n and the \mathbf{k} -vector in the reduced Brillouin zone. Correspondingly, $\hat{\Sigma}$, represents the HF self-energy which mixes spin and valley indices, for details see [71].

To illustrate how our ex-so-tic heterostructure enables to swap two correlated phases, one induced by valley-Zeeman SO and the other by EX coupling, we consider one particular doping level, namely hole density $n_e = -0.183 \cdot 10^{12} \text{ cm}^{-2}$. At positive $V = 18.5 \text{ meV}$, the most stable correlated phase (largest λ_c and largest critical temperature) is a spin-valley coherence SVC $_-$. This phase arises due to the proximity spin-orbit coupling from WS $_2$, and couples the opposite spins at the two valleys. It is characterized by the flat band states close to the Fermi level exhibiting reduced spin polarization, which is not exactly zero because of the residual proximity exchange. Flipping the direction of the displacement field to $V = -18.5 \text{ meV}$, a different correlated phase emerges, CDW $_-$, in which the states at the Fermi level are fully spin-polarized, due to the proximity exchange from CGT.

In Fig. 4 we also show the markedly different quasi-particle Fermi contours of the two swappable phases SVC $_-$ and CDW $_-$. To make this visualization, we plotted thermally broadened density of states (derivative of the Fermi-Dirac function) at $T = 0.4 \text{ K}$:

$$\rho_{n\mathbf{k}} = -\left.\frac{df(\varepsilon)}{d\varepsilon}\right|_{\tilde{\varepsilon}_{n\mathbf{k}}} = \frac{1}{k_B T} \left[4 \cosh\left(\frac{\tilde{\varepsilon}_{n\mathbf{k}} - \mu}{2k_B T}\right)\right]^{-2}. \quad (8)$$

Inspecting Fig. 4 we see that the quasi-particle band structures for the two considered phases, and also

the shapes of their Fermi contours demonstrate very pronounced spectral asymmetries at the corresponding Fermi levels. However, regions with more smeared portions of the Fermi surface (different from just contour plots) are visible in the centre of the reduced Brillouin zone.

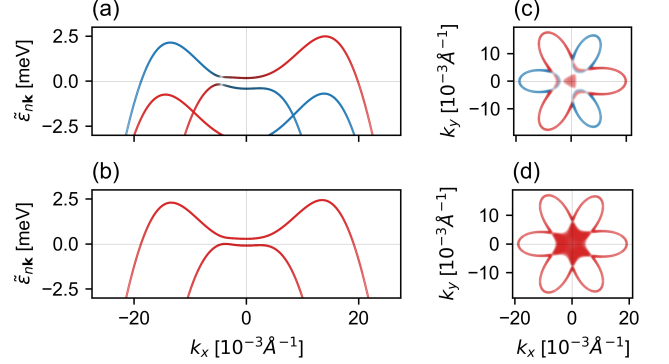


FIG. 4. Swapping SVC and CDW. Calculated HF quasi-particle band structures and spin-valley-resolved Fermi surfaces for the correlated SVC $_-$ phase, panels (a) and (c), with $V = +18.5 \text{ meV}$ and $n_e = -0.183 \cdot 10^{12} \text{ cm}^{-2}$ and CDW $_-$ phase, panels (b) and (d), with $V = -18.5 \text{ meV}$ and $n_e = -0.183 \cdot 10^{12} \text{ cm}^{-2}$. Red, blue, and gray lines mark, correspondingly, spin-up, spin-down, and spin-unpolarized states.

Knowing the HF self-energies $\hat{\Sigma}$ we are able to estimate the magnitudes of the associated correlated gaps, $\Delta_{\hat{\Phi}} = \sum_{s\tau, s'\tau'} \hat{\Phi}_{s'\tau', s\tau}^* \hat{\Sigma}_{s\tau, s'\tau'} / \|\hat{\Phi}\|^2$. This yields for the considered SVP $_-$ and CDW $_-$ phases the following values: $\Delta_{\text{SVP}_-} = 0.109 \text{ meV}$ and $\Delta_{\text{CDW}_-} = 0.085 \text{ meV}$.

To model an interacting system with a symmetry-broken phase at a self-consistent mean-field level, one can factorize \hat{H}_{int} , Eq. (5), in terms of accessible $\hat{\Phi}$'s and for a given dominant phase approximate the interaction just by $\hat{H}_{\Delta} = \Delta_{\hat{\Phi}} \hat{\Phi}$. For example, for a SVC $_{\pm}$ phase, one explores an effective Hamiltonian $\hat{H}_{\text{kin}} + \Delta_{\text{SVC}_{\pm}} \hat{\Phi}_{\text{SVC}_{\pm}}$ which promotes spin-flip-valley-flip hopping due to the interplay of intervalley electron-electron interactions and the valley-Zeeman SO coupling. Such a phase enables novel spin interactions and is expected to result in new phenomena in spintronics [72]. In turn, a CDW $_{\pm}$ phase can be treated on the mean-field level by $\hat{H}_{\text{kin}} + \Delta_{\text{CDW}_{\pm}} \hat{\Phi}_{\text{CDW}_{\pm}}$ which gives rise to spatial modulations of the already spin-split bands due to the proximity-induced EX interaction.

Conclusion. By performing realistic calculations at the RPA level, and by computing Hartree-Fock excitation spectra, we predict that the correlated states of ex-so-tic heterostructures based on BBG can be swapped between SO and EX-driven phases. A single device can exhibit the full spectrum of correlated phases, from uniform Stoner valley polarized, to spatially modulated

spin-polarized CDW and spin-flip-valley-flip spin-valley coherences. While we specifically consider the DFT parametrization of one stacking of WS₂/BBG/CGT, our findings are more general, valid for twisted structures with modified proximity spin interactions, as well as for different encapsulating spin-orbit materials and magnetic semiconductors/insulators.

This work was funded by the Deutsche Forschungsgemeinschaft (DFG, German Research Foundation) SPP 2244 (Project No. 443416183), SFB 1277 (Project-ID 314695032), by the European Union Horizon 2020 Research and Innovation Program under contract number 881603 (Graphene Flagship), and by FLAG-ERA project 2DSOTECH. D.K. acknowledges partial support from the IMPULZ project IM-2021-26—SUPERSPIN funded by the Slovak Academy of Sciences.

* Emails to: iaroslav.zhumagulov@ur.de

† Emails to: denis.kochan@savba.sk

‡ Emails to: jaroslav.fabian@ur.de

- [1] C. R. Dean, L. Wang, P. Maher, C. Forsythe, F. Ghahari, Y. Gao, J. Katoch, M. Ishigami, P. Moon, M. Koshino, T. Taniguchi, K. Watanabe, K. L. Shepard, J. Hone, and P. Kim, *Nature* **497**, 598 (2013).
- [2] Y. Kim, P. Herlinger, P. Moon, M. Koshino, T. Taniguchi, K. Watanabe, and J. H. Smet, *Nano Letters* **16**, 5053 (2016).
- [3] Y. Cao, V. Fatemi, S. Fang, K. Watanabe, T. Taniguchi, E. Kaxiras, and P. Jarillo-Herrero, *Nature* **556**, 43 (2018).
- [4] Y. Cao, V. Fatemi, A. Demir, S. Fang, S. L. Tomarken, J. Y. Luo, J. D. Sanchez-Yamagishi, K. Watanabe, T. Taniguchi, E. Kaxiras, R. C. Ashoori, and P. Jarillo-Herrero, *Nature* **556**, 80 (2018).
- [5] H. Zhou, T. Xie, A. Ghazaryan, T. Holder, J. R. Ehrets, E. M. Spanton, T. Taniguchi, K. Watanabe, E. Berg, M. Serbyn, and A. F. Young, *Nature* **598**, 429 (2021).
- [6] A. L. Szabó and B. Roy, *Phys. Rev. B* **105**, L081407 (2022).
- [7] D.-C. Lu, T. Wang, S. Chatterjee, and Y.-Z. You, *Phys. Rev. B* **106**, 155115 (2022).
- [8] C. Huang, T. M. R. Wolf, W. Qin, N. Wei, I. V. Blinov, and A. H. MacDonald, *Phys. Rev. B* **107**, L121405 (2023).
- [9] F. Winterer, F. R. Geisenhof, N. Fernandez, A. M. Seiler, F. Zhang, and R. T. Weitz, “Ferroelectric and anomalous quantum Hall states in bare rhombohedral trilayer graphene,” (2023), arXiv:2305.04950 [cond-mat.mes-hall].
- [10] F. R. Geisenhof, F. Winterer, A. M. Seiler, J. Lenz, T. Xu, F. Zhang, and R. T. Weitz, *Nature* **598**, 53 (2021).
- [11] H. Zhou, T. Xie, T. Taniguchi, K. Watanabe, and A. F. Young, *Nature* **598**, 434 (2021).
- [12] Y.-Z. Chou, F. Wu, J. D. Sau, and S. Das Sarma, *Phys. Rev. Lett.* **127**, 187001 (2021).
- [13] A. Ghazaryan, T. Holder, M. Serbyn, and E. Berg, *Phys. Rev. Lett.* **127**, 247001 (2021).
- [14] Y.-Z. You and A. Vishwanath, *Phys. Rev. B* **105**, 134524 (2022).
- [15] S. Chatterjee, T. Wang, E. Berg, and M. P. Zaletel, *Nature Communications* **13**, 6013 (2022).
- [16] T. Cea, P. A. Pantaleón, V. T. Phong, and F. Guinea, *Phys. Rev. B* **105**, 075432 (2022).
- [17] W. Qin, C. Huang, T. Wolf, N. Wei, I. Blinov, and A. H. MacDonald, *Phys. Rev. Lett.* **130**, 146001 (2023).
- [18] H. Zhou, L. Holleis, Y. Saito, L. Cohen, W. Huynh, C. L. Patterson, F. Yang, T. Taniguchi, K. Watanabe, and A. F. Young, *Science* **375**, 774 (2022).
- [19] Y. Zhang, R. Polski, A. Thomson, É. Lantagne-Hurtubise, C. Lewandowski, H. Zhou, K. Watanabe, T. Taniguchi, J. Alicea, and S. Nadj-Perge, *Nature* **613**, 268 (2023).
- [20] A. M. Seiler, F. R. Geisenhof, F. Winterer, K. Watanabe, T. Taniguchi, T. Xu, F. Zhang, and R. T. Weitz, *Nature* **608**, 298 (2022).
- [21] Y.-Z. Chou, F. Wu, J. D. Sau, and S. Das Sarma, *Phys. Rev. B* **105**, L100503 (2022).
- [22] S. C. de la Barrera, S. Aronson, Z. Zheng, K. Watanabe, T. Taniguchi, Q. Ma, P. Jarillo-Herrero, and R. Ashoori, *Nature Physics* **18**, 771 (2022).
- [23] L. Holleis, C. L. Patterson, Y. Zhang, H. M. Yoo, H. Zhou, T. Taniguchi, K. Watanabe, S. Nadj-Perge, and A. F. Young, “Ising Superconductivity and Nematicity in Bernal Bilayer Graphene with Strong Spin Orbit Coupling,” (2023), arXiv:2303.00742 [cond-mat.supr-con].
- [24] A. L. Szabó and B. Roy, *Phys. Rev. B* **105**, L201107 (2022).
- [25] Y.-Z. Chou, F. Wu, and S. Das Sarma, *Phys. Rev. B* **106**, L180502 (2022).
- [26] M. Xie and S. Das Sarma, *Phys. Rev. B* **107**, L201119 (2023).
- [27] G. Li, A. Luican, J. M. B. L. dos Santos, A. H. C. Neto, A. Reina, J. Kong, and E. Y. Andrei, *Nature Physics* **6**, 109 (2009).
- [28] R. Bistritzer and A. H. MacDonald, *Proceedings of the National Academy of Sciences* **108**, 12233 (2011).
- [29] F. Zhang, B. Sahu, H. Min, and A. H. MacDonald, *Phys. Rev. B* **82**, 035409 (2010).
- [30] J. F. Sierra, J. Fabian, R. K. Kawakami, S. Roche, and S. O. Valenzuela, *Nature Nanotechnology* **16**, 856 (2021).
- [31] M. Gmitra, S. Konschuh, C. Ertler, C. Ambrosch-Draxl, and J. Fabian, *Phys. Rev. B* **80**, 235431 (2009).
- [32] S. Konschuh, M. Gmitra, D. Kochan, and J. Fabian, *Phys. Rev. B* **85**, 115423 (2012).
- [33] S. Konschuh, M. Gmitra, and J. Fabian, *Phys. Rev. B* **82**, 245412 (2010).
- [34] M. Gmitra, D. Kochan, and J. Fabian, *Phys. Rev. Lett.* **110**, 246602 (2013).
- [35] A. López, L. Colmenárez, M. Peralta, F. Mireles, and E. Medina, *Phys. Rev. B* **99**, 085411 (2019).
- [36] T. Naimer, K. Zollner, M. Gmitra, and J. Fabian, *Phys. Rev. B* **104**, 195156 (2021).
- [37] M. Gmitra and J. Fabian, *Phys. Rev. B* **92**, 155403 (2015).
- [38] M. Gmitra, D. Kochan, P. Högl, and J. Fabian, *Phys. Rev. B* **93**, 155104 (2016).
- [39] K. Zollner and J. Fabian, *Phys. Rev. B* **104**, 075126 (2021).
- [40] K. Zollner, M. Gmitra, and J. Fabian, *Phys. Rev. Lett.* **125**, 196402 (2020).

- [41] K. Zollner, M. Gmitra, and J. Fabian, *Phys. Rev. B* **105**, 115126 (2022).
- [42] K. Zollner, M. Gmitra, T. Frank, and J. Fabian, *Phys. Rev. B* **94**, 155441 (2016).
- [43] H. Haugen, D. Huertas-Hernando, and A. Brataas, *Phys. Rev. B* **77**, 115406 (2008).
- [44] D. Kochan, S. Irmer, and J. Fabian, *Phys. Rev. B* **95**, 165415 (2017).
- [45] K. Zollner and J. Fabian, *Phys. Rev. Lett.* **128**, 106401 (2022).
- [46] J. H. Garcia, M. Vila, A. W. Cummings, and S. Roche, *Chem. Soc. Rev.* **47**, 3359 (2018).
- [47] J. O. Island, X. Cui, C. Lewandowski, J. Y. Khoo, E. M. Spanton, H. Zhou, D. Rhodes, J. C. Hone, T. Taniguchi, K. Watanabe, L. S. Levitov, M. P. Zaletel, and A. F. Young, *Nature* **571**, 85 (2019).
- [48] A. M. Hoque, D. Khokhriakov, K. Zollner, B. Zhao, B. Karpiak, J. Fabian, and S. P. Dash, *Communications Physics* **4**, 124 (2021).
- [49] T. S. Ghiasi, J. Ingla-Aynés, A. A. Kaverzin, and B. J. van Wees, *Nano Letters* **17**, 7528 (2017).
- [50] T. S. Ghiasi, A. A. Kaverzin, P. J. Blah, and B. J. Van Wees, *Nano Lett.* **19**, 5959 (2019).
- [51] C. K. Safeer, J. Ingla-Aynés, F. Herling, J. H. Garcia, M. Vila, N. Ontoso, M. R. Calvo, S. Roche, L. E. Hueso, and F. Casanova, *Nano Letters* **19**, 1074 (2019).
- [52] F. Herling, C. K. Safeer, J. Ingla-Aynés, N. Ontoso, L. E. Hueso, and F. Casanova, *APL Materials* **8**, 071103 (2020).
- [53] T. Wakamura, F. Reale, P. Palczynski, M. Q. Zhao, A. T. C. Johnson, S. Guéron, C. Mattevi, A. Ouerghi, and H. Bouchiat, *Phys. Rev. B* **99**, 245402 (2019).
- [54] T. Wakamura, N. J. Wu, A. D. Chepelianskii, S. Guéron, M. Och, M. Ferrier, T. Taniguchi, K. Watanabe, C. Mattevi, and H. Bouchiat, *Phys. Rev. Lett.* **125**, 266801 (2020).
- [55] J. Ingla-Aynés, F. Herling, J. Fabian, L. E. Hueso, and F. Casanova, *Phys. Rev. Lett.* **127**, 047202 (2021).
- [56] A. A. Kaverzin, T. S. Ghiasi, A. H. Dismukes, X. Roy, and B. J. van Wees, *2D Materials* **9**, 045003 (2022).
- [57] B. Karpiak, A. W. Cummings, K. Zollner, M. Vila, D. Khokhriakov, A. M. Hoque, A. Dankert, P. Svedlindh, J. Fabian, S. Roche, and S. P. Dash, *2D Materials* **7**, 015026 (2019).
- [58] M. Peralta, E. Medina, and F. Mireles, *Phys. Rev. B* **99**, 195452 (2019).
- [59] D. Bohm and D. Pines, *Phys. Rev.* **82**, 625 (1951).
- [60] D. Pines and D. Bohm, *Phys. Rev.* **85**, 338 (1952).
- [61] D. Bohm and D. Pines, *Phys. Rev.* **92**, 609 (1953).
- [62] K. Kuroki, S. Onari, R. Arita, H. Usui, Y. Tanaka, H. Kontani, and H. Aoki, *Phys. Rev. Lett.* **101**, 087004 (2008).
- [63] S. Graser, T. A. Maier, P. J. Hirschfeld, and D. J. Scalapino, *New Journal of Physics* **11**, 025016 (2009).
- [64] T. A. Maier, S. Graser, P. J. Hirschfeld, and D. J. Scalapino, *Phys. Rev. B* **83**, 100515 (2011).
- [65] K. Nomura, S. Ryu, and D.-H. Lee, *Phys. Rev. Lett.* **103**, 216801 (2009).
- [66] T. Wang, M. Vila, M. P. Zaletel, and S. Chatterjee, “Electrical control of spin and valley in spin-orbit coupled graphene multilayers,” (2023), arXiv:2303.04855 [cond-mat.str-el].
- [67] J. M. Koh, J. Alicea, and Étienne Lantagne-Hurtubise, “Correlated phases in spin-orbit-coupled rhombohedral trilayer graphene,” (2023), arXiv:2306.12486 [cond-mat.str-el].
- [68] Y. Zhumagulov, D. Kochan, and J. Fabian, “Emergent correlated phases in rhombohedral trilayer graphene induced by proximity spin-orbit and exchange coupling,” (2023), arXiv:2305.14277 [cond-mat.str-el].
- [69] J. Amann, T. Völkl, T. Rockinger, D. Kochan, K. Watanabe, T. Taniguchi, J. Fabian, D. Weiss, and J. Eroms, *Phys. Rev. B* **105**, 115425 (2022).
- [70] Y.-Z. You and A. Vishwanath, *npj Quantum Materials* **4**, 16 (2019).
- [71] Supplemental material (SM) contains calculational details concerning the irreducible susceptibility χ^0 , Γ vertex function, two-particle response function linear algebra, RPA, self-consistent Hartree-Fock treatment, as well as, details about the correlated low-energy band structures for different broken phases.
- [72] I. Žutić, J. Fabian, and S. Das Sarma, *Rev. Mod. Phys.* **76**, 323 (2004).